

The metallicity extremes of the Sagittarius dSph: SALT spectroscopy of PNe^{*}

Alexei Y. Kniazev,^{1,2,†} Albert A. Zijlstra,^{3,1} Eva K. Grebel,⁴ Leonid S. Pilyugin,⁵ Simon Pustilnik,² Petri Väisänen,¹ David Buckley,¹ Yas Hashimoto,¹ Nicola Loaring,¹ Encarni Romero,¹ Martin Still,¹ Eric B. Burgh,⁶ Kenneth Nordsieck⁶

¹South African Astronomical Observatory, PO Box 9, 7935, Cape Town, South Africa

²Special Astrophysical Observatory, Nizhnij Arkhyz, Karachai-Circassia, 369167, Russia

³University of Manchester, School of Physics & Astronomy, PO Box 88, Manchester M60 1QD

⁴Astronomisches Rechen-Institut, Zentrum für Astronomie Heidelberg, University of Heidelberg, Mönchhofstr. 12–14, D-69120 Heidelberg, Germany

⁵Main Astronomical Observatory of National Academy of Sciences of Ukraine, 27 Zabolotnogo str., 03680 Kiev, Ukraine

⁶Space Astronomy Laboratory, University of Wisconsin, Madison, WI 53706, USA

Accepted 2007 July ?? . Received 2007 June ??; in original form 20?? October ??

ABSTRACT

In this work we present the first spectroscopic results obtained with the Southern African Large Telescope (SALT) telescope during its performance-verification phase. We find that the Sagittarius dwarf spheroidal galaxy (Sgr) Sgr contains a youngest stellar population with $[O/H] \approx -0.2$ and age $t > 1$ Gyr, and an oldest population with $[O/H] = -2.0$. The values are based on spectra of two planetary nebulae (PNe), using empirical abundance determinations. We calculated abundances for O, N, Ne, Ar, S, Cl, Fe, C and He. We confirm the high abundances of PN StWr 2-21 with $12+\log(O/H) = 8.57 \pm 0.02$ dex. The other PN studied, BoBn 1, is an extraordinary object in that the neon abundance exceeds that of oxygen. The abundances of S, Ar and Cl in BoBn 1 yield the original stellar metallicity, corresponding to $12+\log(O/H) = 6.72 \pm 0.16$ dex which is 1/110 of the solar value. The actual $[O/H]$ is much higher: third dredge-up enriched the material by a factor of ~ 12 in oxygen, ~ 240 in nitrogen and ~ 70 in neon. Neon as well as nitrogen and oxygen content may have been produced in the intershell of low-mass AGB stars. Well defined broad WR lines are present in the spectrum of StWr 2-21 and absent in the spectrum of BoBn 1. This puts the fraction of [WR]-type central PNe stars to 67% for dSph galaxies.

Key words: stars: abundances — stars: mass-loss — planetary nebulae: general — galaxies: individual: Sagittarius dwarf spheroidal.

1 INTRODUCTION

The most common morphological type of the dwarf galaxies in the Local Group (LG) are the dwarf spheroidals (dSphs). They are also the least massive, least luminous and most gas-deficient galaxies in the LG. The dSph galaxies are mostly found as satellites of larger galaxies, and their properties are likely affected by their dominant neighbors. The main characteristics are a small size, a lack of interstellar gas and young stars, and a range of metallic-

ities that extend to comparatively high values for their luminosity. The causes of these properties are disputed (Grebel, Gallagher, & Harbeck 2003). Gas-stripping by ram pressure is likely to be involved, and the steep increase of metallicity with age could be caused by removal of the primordial gas reservoir and/or accretion of metal-rich gas from the large neighbour (e.g., Zijlstra et al. 2006).

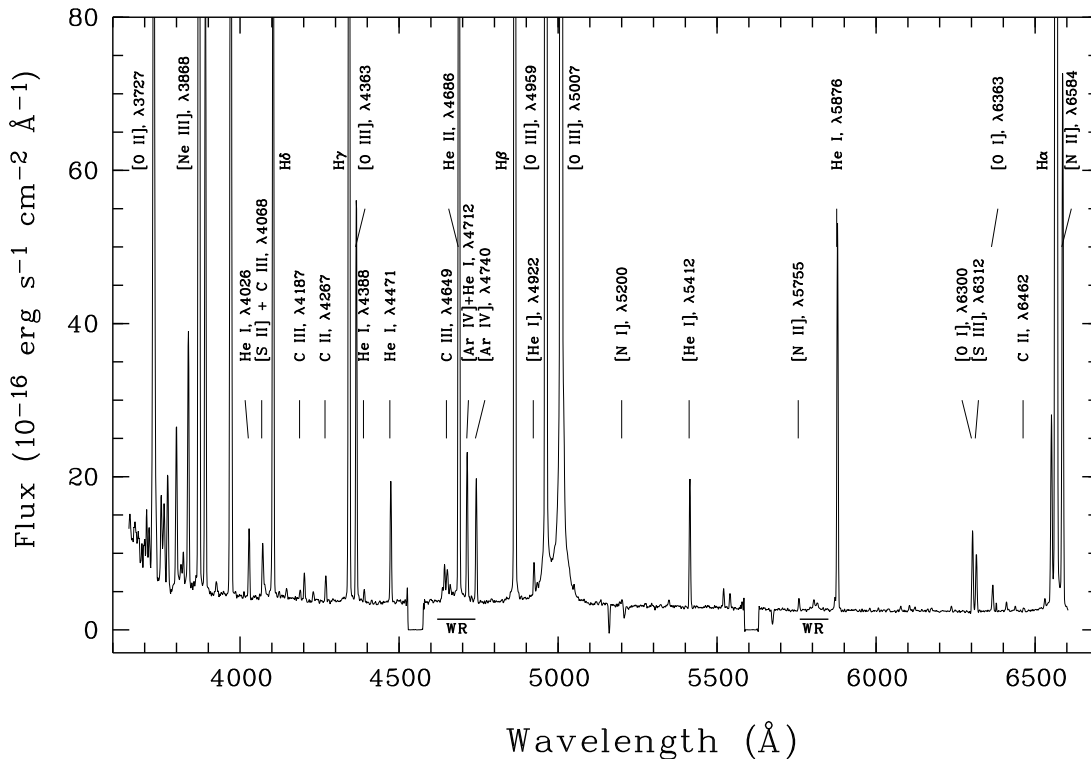
In gas-deficient galaxies, accurate nebular abundances can still be obtained from spectra of planetary nebulae (PNe). These provide information on elements that are not easily observed in stellar absorption-line spectra. For the Local Group and other nearby galaxies these abundance data can also be combined with star formation histories derived from color-magnitude diagrams of resolved stars and ideally with stellar spectroscopic metallicities (e.g., Koch et al.

^{*} Based on observations obtained with South African Large Telescope (SALT).

[†] E-mail: akniazev@saoa.ac.za (AYK); a.zijlstra@manchester.ac.uk (AAZ)

Table 1. Observational details of target PNe

Object Name	Right Ascension J2000	Declination	Date	Exp.time (sec)	Spectral Range (Å)	Slit (arcsec)	V_{\odot} (km s^{-1})
BoBn 1	00 37 16.03	-13 42 58.5	10.10.2006	2×600	3500–6630	1.0	181±4
			13.10.2006	3×600	6000–9030	1.5	187±9
StWr 2-21	19 14 23.35	-32 34 16.6	26.10.2006	2×600	3500–6630	1.0	131±3

**Figure 1.** One-dimensional reduced spectrum of the planetary nebula StWr 2-21. The spectrum covers the wavelength range 3500–6630 Å. Most of the detected stronger emission lines are marked. All detected lines are listed in Table 2. The locations of detected stellar WR lines are also indicated.

2007a,b, and references therein). In turn, this yields deeper insights into galaxy evolution, in particular on the overall chemical evolution of galaxies as a function of time. Only in two dSph galaxies in the LG have PNe been detected and observed to date: two in Fornax (Danziger et al. 1978; Larsen 2008; Kniazev et al. 2007) and four in Sagittarius (Zijlstra & Walsh 1996; Zijlstra et al. 2006).

With a heliocentric distance of ~ 26 kpc to its central region (Monaco et al. 2004), the Sagittarius dwarf is the closest known dSph. Sgr was discovered by Ibata, Gilmore, & Irvin (1994, 1995). It is strongly disrupted by its interaction with the Milky Way (Dohm-Palmer et al. 2001; Helmi & White 2001; Newberg et al. 2003; Majewski et al. 2003; Putman et al. 2004). Since Sgr is located behind the rich stellar population of the Galactic bulge, studies of the stellar population in this galaxy are difficult. Marconi et al. (1998) found that individual stars in Sgr have metallicities in the range $-1.58 \leq [\text{Fe}/\text{H}] \leq -0.71$. Evidence for a more metal-rich population was presented by Bonifacio et al. (2004), who derived $[\text{Fe}/\text{H}] \sim -0.25$ based on spectroscopy of 10 red giant

stars, while Sbordone et al. (2007) have found even higher metallicities between $[\text{Fe}/\text{H}] = -0.9$ and 0. The existence of a significant, much more metal-poor population in Sgr is shown by the metal-poor clusters M 54, Arp 2 and Ter 8 (Layden & Sarajedini 1997, 2000).

Zijlstra & Walsh (1996) discovered two PNe in the Sagittarius dwarf spheroidal galaxy that were previously cataloged as Galactic PNe: Wray 16–423 and He 2–436. The first spectroscopy for them was published by Walsh et al. (1997) and a detailed analysis based on ground-based spectra and radio-continuum data was carried out by Dudziak et al. (2000). Two further PNe were analyzed in Zijlstra et al. (2006): a Sgr-core member, StWr 2-21, and a possible leading-tail member, BoBn 1. The first two PNe showed identical abundances, of $[\text{Fe}/\text{H}] = -0.55 \pm 0.05$ (Walsh et al. 1997; Dudziak et al. 2000). The abundances of the two recent objects are less well defined, being based on less accurate spectroscopy. However, current results indicate that one shows a very high abundance for a dwarf galaxy ($[\text{Fe}/\text{H}] \approx -0.25$), while the other, in contrast, has one of the lowest abundances of any known PN ($[\text{Fe}/\text{H}] \approx -2$). BoBn 1

is located towards a tidal tail (Zijlstra et al. 2006), but its association with Sgr is not as secure as that of the other three; it could also be an unrelated Galactic halo object.

The goal of our present work is to improve our knowledge of the elemental abundances of the last two PNe in the Sagittarius dSph through new high-quality spectra obtained with the new effectively 8-meter diameter Southern African Large Telescope (SALT). The contents of this paper are organized as follows: § 2 gives the description of all observations and data reduction. In § 3 we present our results, and discuss them in § 4. The conclusions drawn from this study are summarized in § 5.

2 OBSERVATIONS AND DATA REDUCTION

2.1 SALT Spectroscopic Observations

The observations of StWr 2-21 and BoBn 1 were obtained during the Performance Verification phase (PV) of the SALT telescope (Buckley, Swart & Meiring 2006; O’Donoghue et al. 2006), and used the Robert Stobie Spectrograph (RSS; Burgh et al. 2003; Kobulnicky et al. 2003). The long-slit spectroscopy mode of the RSS was used, with three mosaiced 2048×4096 CCD detectors. The RSS pixel scale is 0′.129 and the effective field of view is 8′ in diameter. We utilized a binning factor of 2, to give a final spatial sampling of 0′.258 pixel⁻¹. The Volume Phase Holographic (VPH) grating GR900 was used in two spectral ranges: 3500–6600 Å and 5900–8930 Å with a final reciprocal dispersion of ~0.95 Å pixel⁻¹ and spectral resolution FWHM of 5–6 Å. Each exposure was observed with the spectrograph slit aligned to the parallactic angle to avoid loss of light due to atmospheric differential refraction. As shown in Table 1, each exposure was broken up into 2–3 sub-exposures, 10 minutes each, to allow for removal of cosmic rays. Spectra of ThAr and Xe comparison arcs were obtained to calibrate the wavelength scale. Four spectrophotometric standard stars G 93-48, EG 21, BPM 16274 and SA95-42 (Stone & Baldwin 1983; Baldwin & Stone 1984; Massey et al. 1988; Oke 1990) were observed at the parallactic angles for relative flux calibration.

2.2 Data Reduction

The data for each CCD detector were bias and overscan subtracted, gain corrected, trimmed and cross-talk corrected. After that they were mosaiced. The primary data reduction was done using the IRAF¹ package *salt*² developed for SALT data. Cosmic ray removal was done with the task FILTER/COSMIC task in MIDAS.³ We used the IRAF software tasks in *twodspec* package to perform the wavelength

calibration and to correct each frame for distortion and tilt. To derive the sensitivity curve, we fitted the observed spectral energy distribution of the standard stars by a low-order polynomial. All sensitivity curves observed during each night were compared and we found the final curves to have a precision better than 2–3% over the whole optical range, except for the region blueward of λ3700 where precision decreases to 10–15%. Spectra were corrected for the sensitivity curve using the Sutherland extinction curve. One-dimensional (1D) spectra were then extracted using the IRAF APALL task. All one-dimensional spectra obtained with the same setup for the same object were then averaged. Finally, the blue and red parts of the total spectrum of BoBn 1 were combined. The resulting reduced spectra of StWr 2-21 and BoBn 1 are shown in Figure 1 and Figure 2, respectively.

All emission lines were measured applying the MIDAS programs described in detail in Kniazev et al. (2000, 2004): (1) the software is based on the MIDAS Command Language; (2) the continuum noise estimation was done using the absolute median deviation (AMD) estimator; (3) the continuum was determined with the algorithm from Shergin, Kniazev & Lipovetsky (1996); (4) the programs dealing with the fitting of emission/absorption line parameters are based on the MIDAS FIT package; (5) every line was fitted with the Corrected Gauss-Newton method as a single Gaussian superimposed on the continuum-subtracted spectrum. All overlapping lines were fitted simultaneously as a blend of two or more Gaussian features: the [O I] λ6300 and [S III] λ6312, the Hα λ6563 and [N II] λλ6548,6584 lines, the [S II] λλ6716,6731 lines, and the [O II] λλ7320,7330 lines. (6) the final errors in the line intensities, σ_{tot} , include two components: σ_p , due to the Poisson statistics of line photon flux, and σ_c , the error resulting from the creation of the underlying continuum and calculated using the AMD estimator; (7) all uncertainties were then propagated in the calculation of errors in electron number densities, electron temperatures and element abundances.

For the Wolf-Rayet features the Gaussian decomposition to the narrow lines and the broad components was also done using the same method.

SALT is a telescope with a variable pupil, where the illuminating beam changes continuously during the observations. This means that absolute flux calibration is not possible even using spectrophotometric standard stars. To calibrate absolute fluxes we used Hβ fluxes from other sources. For the Hβ flux calibration of BoBn 1 we used the mean value 3.57×10^{-13} erg cm⁻² s⁻¹ calculated from Kwitter & Henry (1996) and Wright, Corradi, & Perinotto (2005) which are in close agreement to each other. The value for the Hβ flux from Peña, Torres-Peimbert, & Ruiz (1991) (2.19×10^{-13} erg cm⁻² s⁻¹) is about 1.5 times weaker compared to the previous references and was ignored for this reason. For the Hβ flux calibration of StWr 2-21 we used the mean value 1.15×10^{-13} erg cm⁻² s⁻¹ from Zijlstra et al. (2006). The resulting spectra in Figure 1 and Figure 2 are shown after this calibration was performed.

2.3 Physical conditions and determination of heavy element abundances

The spectra are interpreted by the technique of plasma diagnostics, i.e. assuming that all lines are produced in an

¹ IRAF: the Image Reduction and Analysis Facility is distributed by the National Optical Astronomy Observatory, which is operated by the Association of Universities for Research in Astronomy, In. (AURA) under cooperative agreement with the National Science Foundation (NSF).

² See <http://www.salt.ac.za/partners-login/partners/data-analysis-software/> for more information.

³ MIDAS is an acronym for the European Southern Observatory package – Munich Image Data Analysis System.

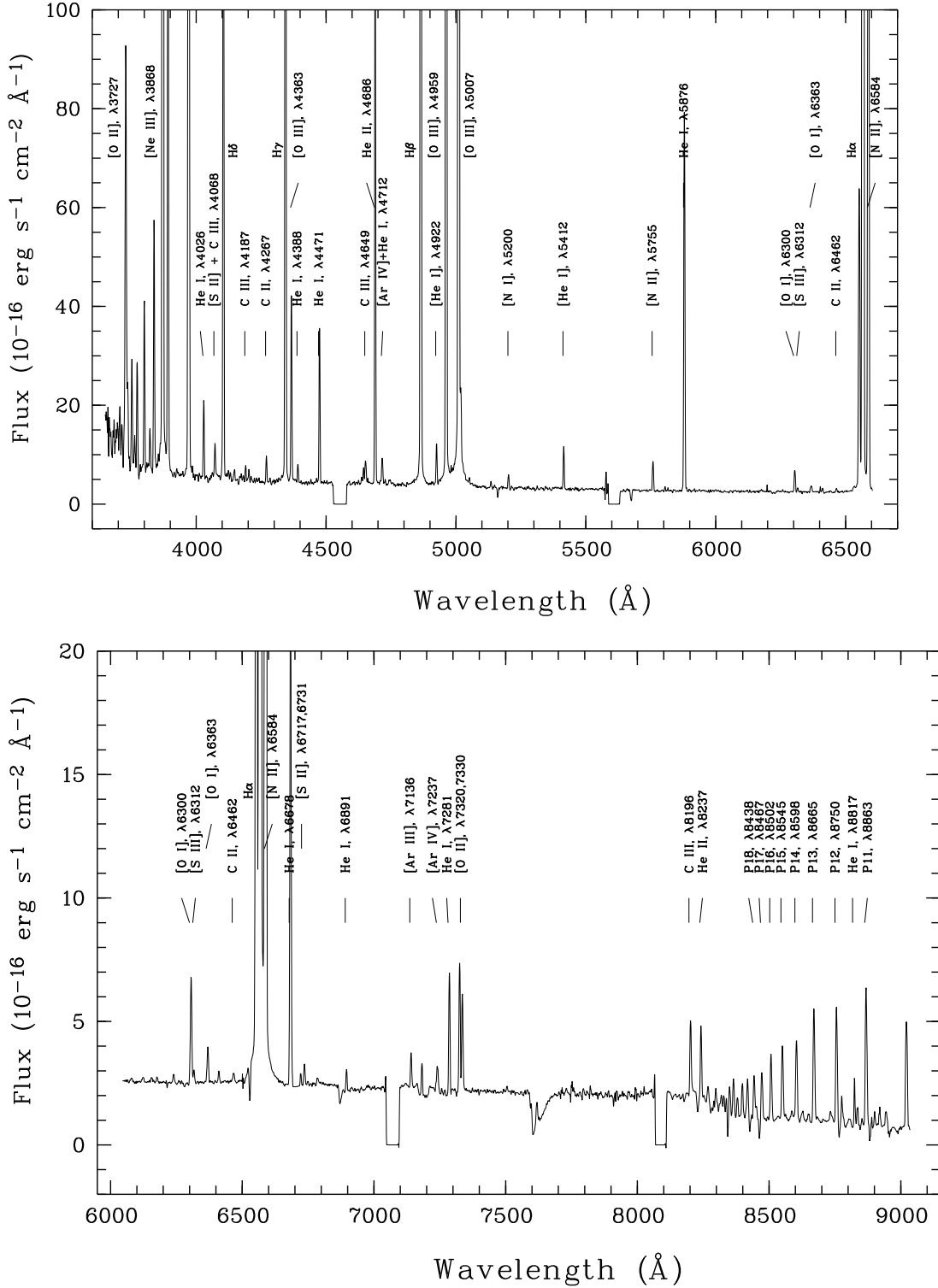


Figure 2. The one-dimensional reduced spectra of the planetary nebula BoBn 1. The top spectrum covers a wavelength range of 3500–6630 \AA and bottom spectrum covers a wavelength range of 6000–9050 \AA . Most of the detected strong emission lines are marked. All detected lines are listed in Table 2.

Table 2. Line intensities of the studied PNe (part I)

$\lambda_0(\text{\AA})$ Ion	StWr 2-21		BoBn 1	
	F(λ)/F(H β)	I(λ)/I(H β)	F(λ)/F(H β)	I(λ)/I(H β)
3727 [O II]	0.3434±0.0119	0.3584±0.0132	0.1638±0.0092	0.1644±0.0095
3750 H12	—	—	0.0343±0.0020	0.0345±0.0021
3771 H11	0.0340±0.0016	0.0354±0.0017	0.0336±0.0023	0.0338±0.0023
3798 H10	0.0500±0.0023	0.0520±0.0025	0.0530±0.0029	0.0532±0.0030
3819 He I	0.0095±0.0015	0.0099±0.0015	0.0157±0.0015	0.0158±0.0016
3835 H9	0.0728±0.0029	0.0756±0.0032	0.0766±0.0031	0.0768±0.0033
3868 [Ne III]	0.7317±0.0236	0.7590±0.0258	2.0668±0.0672	2.0730±0.0710
3889 He I + H8	0.1760±0.0061	0.1824±0.0066	0.2388±0.0087	0.2395±0.0091
3923 He II	0.0041±0.0008	0.0042±0.0008	—	—
3967 [Ne III] + H7	0.3416±0.0108	0.3529±0.0117	0.7299±0.0224	0.7319±0.0236
4026 He I	0.0187±0.0013	0.0193±0.0013	0.0244±0.0012	0.0245±0.0013
4068 [S II] + C III	0.0162±0.0015	0.0166±0.0016	0.0128±0.0012	0.0129±0.0012
4076 [S II]	0.0040±0.0014	0.0042±0.0014	—	—
4101 H δ	0.2483±0.0081	0.2552±0.0086	0.2622±0.0085	0.2628±0.0088
4121 He I	0.0020±0.0010	0.0020±0.0010	—	—
4144 He I	0.0031±0.0011	0.0032±0.0011	0.0035±0.0007	0.0035±0.0007
4187 C III	0.0030±0.0011	0.0030±0.0011	0.0042±0.0007	0.0042±0.0007
4200 He II + N III	0.0072±0.0010	0.0074±0.0011	0.0028±0.0005	0.0028±0.0005
4227 [Fe V]	0.0032±0.0012	0.0033±0.0013	—	—
4267 C II	0.0072±0.0011	0.0074±0.0011	0.0076±0.0006	0.0076±0.0006
4340 H γ	0.4415±0.0144	0.4496±0.0149	0.4699±0.0153	0.4706±0.0156
4363 [O III]	0.1087±0.0039	0.1105±0.0040	0.0561±0.0024	0.0561±0.0024
4388 He I	0.0039±0.0010	0.0039±0.0011	0.0057±0.0007	0.0058±0.0007
4438 He I	—	—	0.0009±0.0003	0.0009±0.0003
4471 He I	0.0332±0.0017	0.0336±0.0017	0.0460±0.0020	0.0461±0.0020
4634 N III	0.0039±0.0022	0.0039±0.0022	0.0021±0.0014	0.0021±0.0014
4640 N III	0.0100±0.0023	0.0101±0.0023	0.0050±0.0014	0.0050±0.0014
4649 C III	0.0115±0.0033	0.0115±0.0034	0.0094±0.0021	0.0094±0.0021
4658 [Fe III]	0.0053±0.0032	0.0053±0.0032	0.0013±0.0008	0.0013±0.0008
4686 He II	0.4177±0.0127	0.4202±0.0128	0.1738±0.0055	0.1739±0.0055
4712 [Ar IV] + He I	0.0397±0.0026	0.0399±0.0026	0.0087±0.0014	0.0087±0.0014
4740 [Ar IV]	0.0326±0.0025	0.0328±0.0025	0.0017±0.0014	0.0017±0.0014
4861 H β	1.0000±0.0309	1.0000±0.0309	1.0000±0.0315	1.0000±0.0315
4922 He I	0.0133±0.0018	0.0132±0.0018	0.0117±0.0008	0.0117±0.0008
4959 [O III]	3.5942±0.1217	3.5829±0.1214	1.1543±0.0390	1.1540±0.0391
5007 [O III]	10.3838±0.3345	10.3353±0.3335	3.4256±0.1102	3.4242±0.1103
5048 He I	—	—	0.0016±0.0003	0.0016±0.0003
5131 O I	—	—	0.0021±0.0005	0.0021±0.0005
5200 [N I]	0.0018±0.0012	0.0018±0.0012	0.0045±0.0006	0.0045±0.0006
5412 He II	0.0329±0.0015	0.0324±0.0015	0.0131±0.0008	0.0130±0.0008
5518 [Cl III]	0.0045±0.0009	0.0044±0.0008	0.0001±0.0001	0.0001±0.0001
5538 [Cl III]	0.0037±0.0010	0.0036±0.0010	0.0002±0.0001	0.0002±0.0001
5755 [N II]	0.0032±0.0012	0.0031±0.0012	0.0103±0.0007	0.0103±0.0007
5801 C IV	0.0021±0.0012	0.0020±0.0012	—	—
5812 C IV	0.0012±0.0011	0.0012±0.0011	0.0006±0.0002	0.0006±0.0002
5869 He II	0.0035±0.0012	0.0034±0.0012	—	—
5876 He I	0.1027±0.0034	0.0997±0.0034	0.1318±0.0044	0.1314±0.0045
6074 He II	0.0010±0.0005	0.0009±0.0005	—	—
6102 [K IV]	0.0014±0.0008	0.0013±0.0008	—	—
6118 He II	0.0007±0.0004	0.0007±0.0004	—	—
6234 He II	0.0013±0.0008	0.0012±0.0008	—	—
6300 [O I]	0.0225±0.0015	0.0216±0.0014	0.0085±0.0004	0.0085±0.0004
6312 [S III]	0.0161±0.0012	0.0154±0.0012	0.0013±0.0002	0.0013±0.0002
6364 [O I]	0.0077±0.0012	0.0074±0.0012	0.0030±0.0008	0.0030±0.0008
6406 He II	0.0024±0.0011	0.0023±0.0010	0.0009±0.0003	0.0009±0.0003
6435 [Ar V]	0.0011±0.0007	0.0011±0.0007	—	—
6462 C II	0.0008±0.0009	0.0007±0.0009	0.0010±0.0004	0.0010±0.0004
6527 He II	0.0028±0.0010	0.0026±0.0010	—	—

Table 3. Line intensities of the studied PNe (part II)

$\lambda_0(\text{\AA})$ Ion	StWr 2-21		BoBn 1	
	$F(\lambda)/F(\text{H}\beta)$	$I(\lambda)/I(\text{H}\beta)$	$F(\lambda)/F(\text{H}\beta)$	$I(\lambda)/I(\text{H}\beta)$
6548 [N II]	0.0609±0.0165	0.0581±0.0158	0.1378±0.0041	0.1373±0.0045
6563 H α	2.9783±0.0902	2.8448±0.0936	2.7786±0.0839	2.7680±0.0908
6584 [N II]	0.1651±0.0197	0.1577±0.0189	0.4134±0.0166	0.4118±0.0174
6678 He I	0.0265±0.0012 ^a	0.0252±0.0012	0.0396±0.0012	0.0394±0.0013
6717 [S II]	0.0200±0.0009 ^a	0.0190±0.0009	0.0009±0.0001	0.0009±0.0001
6731 [S II]	0.0297±0.0014 ^a	0.0283±0.0014	0.0017±0.0001	0.0016±0.0001
6891 He II	—	—	0.0015±0.0005	0.0015±0.0005
7065 He I	0.0233±0.0017 ^a	0.0220±0.0017	—	—
7136 [Ar III]	0.0936±0.0069 ^a	0.0884±0.0066	0.0026±0.0006	0.0025±0.0005
7178 He II	—	—	0.0023±0.0006	0.0023±0.0006
7237 [Ar IV]	—	—	0.0025±0.0004	0.0025±0.0004
7281 He I	—	—	0.0093±0.0007	0.0092±0.0008
7320 [O II]	—	—	0.0104±0.0004	0.0103±0.0004
7330 [O II]	—	—	0.0078±0.0004	0.0077±0.0004
7500 He I	—	—	0.0005±0.0005	0.0005±0.0005
8196 C III	—	—	0.0063±0.0006	0.0062±0.0006
8237 He II	—	—	0.0057±0.0007	0.0056±0.0007
8359 P22 + C III	—	—	0.0032±0.0006	0.0032±0.0006
8374 P21	—	—	0.0017±0.0006	0.0016±0.0006
8392 P20	—	—	0.0030±0.0007	0.0030±0.0007
8413 P19	—	—	0.0034±0.0005	0.0033±0.0005
8437 P18	—	—	0.0041±0.0004	0.0041±0.0004
8467 P17	—	—	0.0044±0.0009	0.0044±0.0009
8502 P16	—	—	0.0060±0.0008	0.0060±0.0009
8545 P15	—	—	0.0073±0.0009	0.0072±0.0009
8598 P14	—	—	0.0080±0.0009	0.0079±0.0009
8665 P13	—	—	0.0112±0.0009	0.0111±0.0010
8750 P12	—	—	0.0110±0.0009	0.0109±0.0010
8817 He I	—	—	0.0029±0.0005	0.0029±0.0005
8863 P11	—	—	0.0142±0.0011	0.0141±0.0011
C(H β) dex	0.06±0.04		0.01±0.04	
EW(H β) Å	671±15		900±20	

^a intensity was taken from Zijlstra et al. (2006).

isothermal gas at uniform density and ionization level. As a first step, the reddening correction, electron temperatures and density were calculated. These steps are repeated several times, until the values converge.

The measured emission line intensities $F(\lambda)$ were corrected for reddening using the equation

$$\frac{I(\lambda)}{I(\text{H}\beta)} = \frac{F(\lambda)}{F(\text{H}\beta)} \cdot 10^{C(\text{H}\beta)f(\lambda)}, \quad (1)$$

where $C(\text{H}\beta)$ is the extinction coefficient, $I(\lambda)$ is the intrinsic line flux and $F(\lambda)$ is the observed line flux corrected for atmospheric extinction. $f(\lambda)$ is the reddening function, taken from Whitford (1958) and normalized at H β . Izotov, Thuan, & Lipovetsky (1994) noted that this reddening function can be approximated over the whole spectral range with an accuracy better than 5% by

$$f(\lambda) = 3.15854 \cdot 10^{-1.02109\lambda} - 1 \quad (2)$$

where λ is in units of μm . The Balmer theoretical ratios from Brocklehurst (1971) were used with equation 1 in an iterative way for the intrinsic hydrogen line intensity ratios for estimated electron temperature.

For collisionally excited lines (CELs), we calculated ionic and total element abundances for O, N, S, Ne, Ar, Cl and Fe using equations from Izotov et al. (2006). These recent equations are based on sequences of photoionization models and used the new atomic data of Stasińska (2005).

Izotov et al. (2006) find that the electron temperature $T_e(\text{O III})$ derived from the [O III] ($\lambda 4959 + \lambda 5007$)/ $\lambda 4363$ line ratio using old and new emissivities differ by less than 1% in the temperature range 5000–20,000 K. For this reason the electron temperature $T_e(\text{O III})$ was derived from an iterative procedure, using the equation from Aller (1984):

$$\frac{I(4959 + 5007)}{I(4363)} = C_T \left[\frac{1 + a_1 x}{1 + a_2 x} \right] 10^{1.432/t}, \quad (3)$$

where $t = 10^{-4} T_e(\text{O III})$ and $x = 10^{-4} N_e t^{-0.5}$. The parameters C_T , a_1 , a_2 were calculated using the following interpolations:

$$C_T = 8.44 - 1.09t + 0.5t^2 - 0.08t^3, \quad (4)$$

$$a_1 = 2 \cdot 10^{-4} + 3.13 \cdot 10^{-4}t - 1.6 \cdot 10^{-4}t^2 + 2.67 \cdot 10^{-5}t^3, \quad (5)$$

$$a_2 = 0.0291 + 0.0253t - 0.0128t^2 + 0.00213t^3 \quad (6)$$

Table 4. Important line ratios, calculated temperatures and electron densities in studied PNe

Value	StWr 2-21	BoBn 1
[O III] ($\lambda 4959 + \lambda 5007$)/ $\lambda 4363$	127.88 \pm 5.73	81.72 \pm 4.04
[N II] ($\lambda 6548 + \lambda 6584$)/ $\lambda 5755$	69.12 \pm 5.18	53.28 \pm 2.06
[S II] $\lambda 6731/\lambda 6717$	0.674 \pm 0.045	0.520 \pm 0.056
[Cl III] $\lambda 5518/\lambda 5538$	1.222 \pm 0.414	0.594 \pm 1.548
[Ar IV] $\lambda 4711/\lambda 4740$	1.116 \pm 0.109 ^a	—
$T_e(\text{O III})(\text{K})$	11700 \pm 190	13720 \pm 870
$T_e(\text{N II})(\text{K})$	11360 \pm 2200	11320 \pm 1630
$T_e(\text{Ar III})(\text{K})$	12050 \pm 340	13250 \pm 1330
$T_e(\text{Cl III})(\text{K})$	12050 \pm 340	13250 \pm 1330
$N_e(\text{S II } \lambda 6731/\lambda 6717)$	2700 ⁺⁸⁵⁰ ₋₅₇₀	9600 ⁺²⁷¹⁰⁰ ₋₄₃₆₀
$N_e(\text{Cl III } \lambda 5518/\lambda 5538)$	930 ⁺⁴⁴⁵⁰ ₋₉₃₀	13400: ^a
$N_e(\text{Ar IV } \lambda 4711/\lambda 4740)^b$	2920 ⁺¹⁵⁴⁰ ₋₁₂₂₀	—

^a Has large errors.

^b Corrected for the He I $\lambda 4713$ line.

The density N_e was also derived iteratively, using the [S II] $\lambda 6717/\lambda 6731$ line ratio. The [O III] auroral $\lambda 4363$ line was corrected for recombination excitation following the equation from Liu et al. (2000).

The line [N II] $\lambda 5755$ was detected in the spectra of both studied PNe, which allowed us to determine $T_e(\text{N II})$ directly from the $Q_N = [\text{N II}] (\lambda 6548 + \lambda 6584)/\lambda 5755$ line ratio. It is convenient to have an analytic expression linked the electron temperature $T_e(\text{N II})$ to the value of the Q_N and the electron density N_e . To establish such a relation we have obtained the five-level-atom solution for the N^+ ion, with a recent atomic data. The Einstein coefficients for spontaneous transitions and the energy levels for five low-lying levels were taken from Galavís, Mendoza & Zeippen (1997). The effective cross sections or effective collision strengths for electron impact were taken from Hudson & Bell (2005). The effective cross sections are continuous functions of temperatures, tabulated by Hudson & Bell (2005) at a fixed temperatures. The actual effective cross sections for a given electron temperature are derived from two-order polynomial fits of the data from Hudson & Bell (2005) as a function of temperature.

We derived a numerical solution of the five-level-atom for a large range of values of electron temperature (within the range 5,000 \div 25,000 K) and of electron density (within the range 10 \div 10⁶ cm⁻³). The analytic relation was derived as an approximation of those numerical results. The following simple expression for the approximation was adopted (this type of expression was widely used by different authors)

$$t = \frac{C_0}{\log(Q_N) + C_1 + C_2 \log(t) + C_3 t} \quad (7)$$

where $t = 10^{-4}T_e(\text{N II})$ and coefficients C_i can be a function of the electron density. At $N_e \lesssim 10^3$ cm⁻³ the coefficients C_i are, in fact, independent of N_e , and the numerical results are well reproduced by the relation

Table 5. Elemental abundances in studied PNe

Value	StWr 2-21	BoBn 1
$\text{O}^+/\text{H}^+(\times 10^5)$	1.14 \pm 0.87	0.88 \pm 0.93
$\text{O}^{++}/\text{H}^+(\times 10^5)$	22.85 \pm 1.26	4.76 \pm 0.83
$\text{O}^{+++}/\text{H}^+(\times 10^5)$	12.75 \pm 1.09	0.78 \pm 0.18
$\text{O}/\text{H}(\times 10^5)$	36.75 \pm 1.88	6.42 \pm 1.26
12+log(O/H)	8.57 \pm 0.02	7.81 \pm 0.09
$\text{N}^+/\text{H}^+(\times 10^7)$	23.06 \pm 11.13	63.48 \pm 24.38
ICF(N)	23.842	6.837
$\text{N}/\text{H}(\times 10^5)$	5.50 \pm 2.65	4.34 \pm 1.67
12+log(N/H)	7.74 \pm 0.21	7.64 \pm 0.17
log(N/O)	-0.83 \pm 0.21	-0.17 \pm 0.18
$\text{Ne}^{++}/\text{H}^+(\times 10^5)$	4.55 \pm 0.31	7.26 \pm 1.47
ICF(Ne)	1.437	1.110
$\text{Ne}/\text{H}(\times 10^5)$	6.54 \pm 0.44	8.06 \pm 1.64
12+log(Ne/H)	7.82 \pm 0.03	7.91 \pm 0.09
log(Ne/O)	-0.75 \pm 0.04	0.10 \pm 0.12
$\text{S}^+/\text{H}^+(\times 10^7)$	1.06 \pm 0.46	0.09 \pm 0.09
$\text{S}^{++}/\text{H}^+(\times 10^7)$	16.67 \pm 2.14	0.99 \pm 0.38
ICF(S)	5.538	1.324
$\text{S}/\text{H}(\times 10^7)$	98.21 \pm 12.11	1.44 \pm 0.52
12+log(S/H)	6.99 \pm 0.05	5.16 \pm 0.16
log(S/O)	-1.57 \pm 0.06	-2.65 \pm 0.18
$\text{Ar}^{++}/\text{H}^+(\times 10^7)$	5.66 \pm 0.54	0.15 \pm 0.06
$\text{Ar}^{+++}/\text{H}^+(\times 10^7)$	6.76 \pm 0.51	0.22 \pm 0.17
ICF(Ar)	1.067	1.002
$\text{Ar}/\text{H}(\times 10^7)$	13.25 \pm 0.80	0.37 \pm 0.19
12+log(Ar/H)	6.12 \pm 0.03	4.57 \pm 0.22
log(Ar/O)	-2.44 \pm 0.03	-3.24 \pm 0.23
$\text{Fe}^{++}/\text{H}^+(\times 10^7)$	2.18 \pm 1.60	0.54 \pm 0.38
ICF(Fe)	35.185	9.786
log(Fe/O)	-1.68 \pm 0.32	-2.09 \pm 0.31
[Fe/H]	-0.66 \pm 0.32	-1.82 \pm 0.30
[O/Fe]	0.46 \pm 0.32	0.87 \pm 0.30
$\text{Cl}^{++}/\text{H}^+(\times 10^8)$	2.92 \pm 0.52	0.08 \pm 0.04
ICF(Cl)	4.287	1.690
$\text{Cl}/\text{H}(\times 10^8)$	12.50 \pm 2.23	0.14 \pm 0.07
12+log(Cl/H)	5.10 \pm 0.08	3.14 \pm 0.23
log(Cl/O)	-3.47 \pm 0.08	-4.66 \pm 0.24
$\text{He}^+/\text{H}^+(\times 10^2)$	6.99 \pm 0.18	8.52 \pm 0.40
$\text{He}^{++}/\text{H}^+(\times 10^2)$	3.61 \pm 0.11	1.53 \pm 0.05
$\text{He}/\text{H}(\times 10^2)$	10.60 \pm 0.21	10.05 \pm 0.41
12+log(He/H)	11.03 \pm 0.01	11.00 \pm 0.02
$\text{C}^{++}/\text{H}^+(\times 10^4)$	7.27 \pm 1.18	7.78 \pm 0.67
$\text{C}^{+++}/\text{H}^+(\times 10^4)$	5.14 \pm 1.23	5.62 \pm 0.48
ICF(C)	1.050	1.184
$\text{C}/\text{H}(\times 10^4)$	13.03 \pm 1.78	15.86 \pm 0.98
12+log(C/H)	9.11 \pm 0.06	9.20 \pm 0.03
log(C/O)	0.55 \pm 0.06	1.39 \pm 0.09

$$t = \frac{1.111}{\log(Q_N) - 0.892 - 0.144 \log(t) + 0.023 t} \quad (8)$$

derived by Pilyugin (2007) for $N_e = 100$ cm⁻³. At $N_e \gtrsim 10^3$ cm⁻³ the dependence of the coefficients C_i on the electron density are reproduced by the following relations

$$C_0 = 2.56604 - 1.04750 w + 0.23621 w^2 - 0.01608 w^3, \quad (9)$$

$$C_1 = 2.94332 - 2.53546 w + 0.48115 w^2 - 0.01988 w^3, \quad (10)$$

$$C_2 = -9.03905 + 6.89003 w - 1.68270 w^2 + 0.12347 w^3, \quad (11)$$

$$C_3 = 0.70472 - 0.55891 w + 0.14310 w^2 - 0.01084 w^3, \quad (12)$$

where $w = \log(N_e)$. The values of $T_e(\text{N II})$ derived directly from the numerical solution and with the approximation differ by less than 3% at $N_e \lesssim 10^5 \text{ cm}^{-3}$ and by around around 5% at $N_e \sim 10^6 \text{ cm}^{-3}$ and $t \sim 2.5$. It should be emphasized that at $N_e \lesssim 10^3 \text{ cm}^{-3}$ Eqs.(9)-(12) are not workable, and Eq.(8) should be used in this case.

We thus used $T_e(\text{N II})$ from Eq.(7) for the calculation of N^+/H^+ , O^+/H^+ , S^+/H^+ and $\text{Fe}^{2+}/\text{H}^+$ abundances. We calculated also $T_e(\text{O II})$ and $T_e(\text{S III})$ using approximations from Izotov et al. (2006). We used $T_e(\text{S III})$ for the calculation of S^{2+}/H^+ , $\text{Cl}^{2+}/\text{H}^+$ and $\text{Ar}^{2+}/\text{H}^+$ abundances and $T_e(\text{O III})$ from Eq.(3) for the calculation of O^{2+}/H^+ and $\text{Ne}^{2+}/\text{H}^+$ abundances.

For StWr 2-21 only the $[\text{O II}] \lambda\lambda 3727, 3729$ doublet was used to calculate O^+/H^+ . In case of BoBn 1, O^+/H^+ was calculated as a weighted average of O^+/H^+ using intensities of the $[\text{O II}] \lambda\lambda 3727, 3729$ doublet as well as using the $[\text{O II}] \lambda\lambda 7320, 7330$ lines. The contribution to the intensities of the $[\text{O II}] \lambda\lambda 7320, 7330$ lines due to recombination was taken into account following the correction from Liu et al. (2000).

The detection of a strong nebular $\text{He II} \lambda 4686$ emission implies the presence of a non-negligible amount of O^{3+} . In this case its abundance is derived from the relation:

$$\frac{\text{O}^{3+}}{\text{H}^+} = \frac{\text{He}^{2+}}{\text{He}^+} \left(\frac{\text{O}^+}{\text{H}^+} + \frac{\text{O}^{2+}}{\text{H}^+} \right) \quad (13)$$

After that, the total oxygen abundance is equal to

$$\frac{\text{O}}{\text{H}} = \frac{\text{O}^+}{\text{H}^+} + \frac{\text{O}^{2+}}{\text{H}^+} + \frac{\text{O}^{3+}}{\text{H}^+} \quad (14)$$

From measured intensities of optical recombination lines (ORLs), ionic abundances were calculated using the equation:

$$\frac{N(\text{X}^{i+})}{N(\text{H}^+)} = \frac{I_{\text{jk}}}{I_{\text{H}\beta}} \frac{\lambda_{\text{jk}}}{\lambda_{\text{H}\beta}} \frac{\alpha_{\text{H}\beta}}{\alpha_{\text{jk}}} \quad (15)$$

where $I_{\text{jk}}/I_{\text{H}\beta}$ is the intensity ratio of the ionic line to the $\text{H}\beta$ line, $\lambda_{\text{jk}}/\lambda_{\text{H}\beta}$ is the wavelength ratio of the ionic line to $\text{H}\beta$, $\alpha_{\text{H}\beta}$ is the effective recombination coefficient for $\text{H}\beta$ and α_{jk} is the effective recombination coefficient for the ionic ORL. Ionic abundances derived from optical recombination lines (ORLs) depend only weakly on the adopted temperature and are essentially independent of N_e . A temperature of $T_e(\text{O III})$ was assumed throughout. The ionic abundance of observed C II recombination lines was derived using calculated effective recombination coefficients from Davey, Storey & Kisielius (2000), which include both radiative and dielectronic recombination processes. The ionic abundance of observed C III recombination lines was derived using effective recombination coefficients from Péquignot, Petitjean, & Boisson (1991). The effective recombination coefficient for $\text{H}\beta$ was taken from Péquignot et al. (1991) as well. Dielectronic recombination coefficients for C III lines were taken from Nussbaumer & Storey (1984). ICF for C were calculated using Kingsburg & Barlow (1994).

Helium was calculated in the manner described in Izotov, Thuan, & Lipovetsky (1997); Izotov & Thuan (1998, 2004). The new Benjamin, Skillman & Smith (2002) fits were used to convert He I emission line strengths to singly ionized helium $y^+ = \text{He}^+/\text{H}^+$ abundances.

The $[\text{Cl III}] \lambda 5518/\lambda 5538$ line ratio and $[\text{Ar IV}] \lambda 4711/\lambda 4740$ line ratio were also used to calculate the density for StWr 2-21. The TEMDEN task contained within the IRAF NEBULAR package was used in this case. Since $[\text{Ar IV}] \lambda 4711$ is contaminated by the He I $\lambda 4713$ line, we have subtracted the latter adopting a He I $\lambda 4713/\lambda 4471$ recombination ratio (Brocklehurst 1972) that could be approximated for T_e varying between 10,000 and 20,000 K with a linear equation:

$$\frac{\text{He I } \lambda 4713}{\text{He I } \lambda 4471} = 0.045 + 0.047 t \quad (16)$$

Unfortunately, these lines are very weak and have large errors in case of BoBn 1.

3 RESULTS

The measured heliocentric radial velocities for the two studied PNe are given in Table 1. The two independent measurements for BoBn 1 are consistent with each other and all measured velocities are consistent within the uncertainties with velocities published in Zijlstra et al. (2006).

Tables 2 and 3 list the relative intensities of all detected emission lines relative to $\text{H}\beta$ ($F(\lambda)/F(\text{H}\beta)$), the ratios corrected for the extinction ($I(\lambda)/I(\text{H}\beta)$), as well as the derived extinction coefficient $C(\text{H}\beta)$, and the equivalent width of the $\text{H}\beta$ emission line $\text{EW}(\text{H}\beta)$. $C(\text{H}\beta)$ combines the internal extinction in each PN and the foreground extinction in the Milky Way, however internal extinction tends to be low in all but the youngest PNe. The electron temperatures $T_e(\text{O III})$, $T_e(\text{N II})$, the number densities $N_e(\text{S II})$, $N_e(\text{Ar IV})$, $N_e(\text{Cl III})$ are shown in Table 4 together with the line ratios that were used for their calculations. The ionic and total element abundances and ICFs for O, N, Ne, S, Ar, Fe, Cl, C and He are presented in Table 5.

It is desirable to compare densities derived from diagnostics that are observed in the same spectrum, in order to compare the same volume in the nebula. Stanghellini & Kaler (1989) examined densities derived for a large sample of PNe and have found that densities derived from the $[\text{O II}]$, $[\text{S II}]$, $[\text{Ar IV}]$ and $[\text{Cl III}]$ doublet ratios agree to within $\sim 30\%$. Kingsburg & English (1992) studied a sample of 57 PNe having densities in the range 500–10000 sm^{-3} and showed that $N_e(\text{O II})$ and $N_e(\text{S II})$ are the same within the errors. As seen from Table 4, both PNe have densities that are equal within the formal observational errors and we may conclude that the nebulae are roughly homogeneous.

The comparison of measured line intensities for StWr 2-21 with those published by Zijlstra et al. (2006) show good agreement, within the cited errors. Our RSS spectra have a spectral resolution of 5–6 Å, which is about two times better than the spectral resolution of 11 Å Zijlstra et al. (2006) obtained with EFOSC2 on the ESO 3.6m telescope. This allows for a more accurate detection of faint lines in the same spectral region and the possibility to fit in detail (see Figure 1) both the blue and the red WR bumps clearly evident

in our spectrum (see Section 3.1 for more details). There are many weak He lines detected in the spectrum of StWr 2-21, especially in the spectral region 5800–6550 Å. Since our observed spectral region for StWr 2-21 is limited to $< 6630\text{Å}$ and our detected intensities for the relatively bright lines are very similar to those cited in Zijlstra et al. (2006, see their Table 2), we additionally used those spectral data (for $\lambda > 6630\text{Å}$) in our calculations of abundances of S, Ar and He. All these lines are marked in Table 3. The determined abundances of various elements using the SALT spectrum are fairly consistent with those published by Zijlstra et al. (2006) that have been obtained from models. Zijlstra et al. (2006) did not determine errors on their abundances. Our data also allows us, for the first time, to determine abundances of Fe and Cl in StWr 2-21.

Torres-Peimbert & Peimbert (1979), Barker (1980), Peña et al. (1991) and Wright et al. (2005) carried out previous spectroscopic observations of BoBn 1 PN using KPNO 2.1m, CTIO 4-m and INT 2.5m telescopes. Our data for BoBn 1 are considerably better than the earlier spectra, in terms of signal-to-noise ratio, resolution and spectral coverage, yielding a signal-to-noise ratio, for example, of 23 for the [O III] $\lambda 4363$ line. With our new SALT data we securely detect, for the first time, the weak [S II] $\lambda\lambda 6717, 6731$ lines ($I(6717+6731) \approx 0.0025 I(H\beta)$) and determine the electron number density to be three times as large as found before (Torres-Peimbert & Peimbert 1979; Peña et al. 1991). Unfortunately, even with our data the errors for [S II] $\lambda\lambda 6717, 6731$ lines are still large, yielding large errors for the density. This leads to significant errors of practically all calculated abundances based on CELs. Our abundances for BoBn 1 are consistent within the uncertainties cited by (Peña et al. 1991). Abundances for BoBn 1 have been also obtained by Howard, Henry, & McCartney (1997) and by Zijlstra et al. (2006) from models. However, both papers are based on the previous observational data (mainly from Peña et al. 1991), where the most important lines for determination of Ar, S and C were obtained with large uncertainties, the [N II] $\lambda 5755$ line was outside of the observed spectral region and [S III] $\lambda 6312$ was not detected.

The dichotomy between the ORL and CEL abundances is a well known problem in nebular astrophysics (see Liu 2003, and references therein). Heavy-element abundances derived from ORLs are systematically higher than those derived from CELs. Torres-Peimbert & Peimbert (1979) calculated the abundance of C for BoBn 1 using the ultraviolet C III] $\lambda 1909$, comparing it with the C abundance calculated from optical recombination lines and found agreement. Our total C abundance (see Table 5) derived using the five ORL C II and C III lines is consistent, within the quoted uncertainties, with their value of $12+\log(C/H) = 9.16 \pm 0.15$. Unfortunately, there were no ORL lines detected for other elements and we have to conclude that a higher S/N spectrum will be needed to identify any discrepancy between the ORL and CEL abundances for both StWr 2-21 and BoBn 1.

3.1 Wolf-Rayet features

Zijlstra et al. (2006) reported a detection, based on spectral synthesis, of two broad Wolf-Rayet (WR) features at 3820 and 5805 Å in their StWr 2-21 spectrum. There is confirming evidence in our SALT data of broad blue (4640–4750 Å)

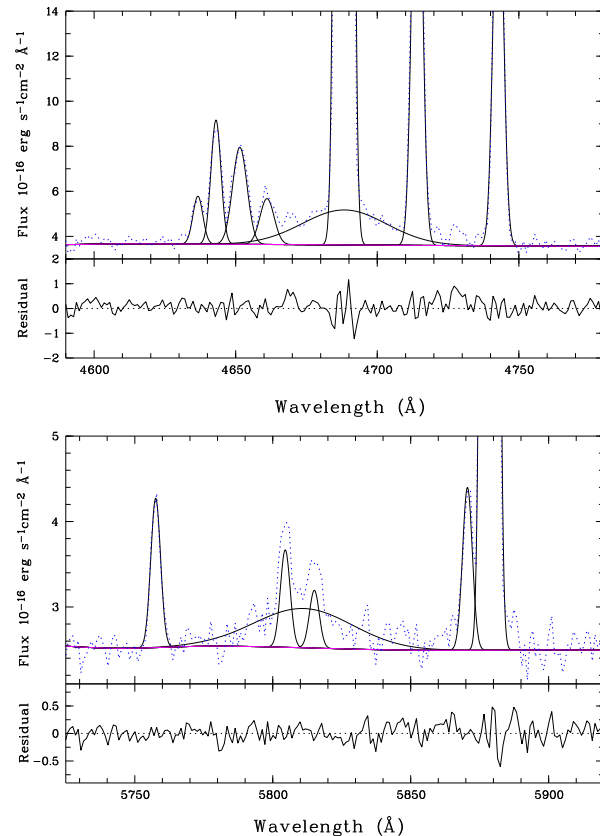


Figure 3. Gaussian multicomponent fitting of the blue (top) and the red (bottom) Wolf-Rayet bumps of StWr 2-21. In the top part of each panel the observed spectrum in the fitted region (dashed lines), fitted Gaussians and created continuum level are shown. In the bottom part of each panel residuals between the observed spectrum and the continuum plus fitted lines are plotted. The following lines from left to right are separated: *Top panel:* The narrow lines (FWHM=4.1 Å) N III $\lambda 4634$, N III $\lambda 4640$, C III $\lambda\lambda 4647+4650$, [Fe III] $\lambda 4658$, He II $\lambda 4686$ (narrow and broad components), narrow [Ar IV]+He II $\lambda\lambda 4711+4713$, and [Ar IV] $\lambda 4740$; *Bottom panel:* The narrow lines (FWHM=5.15 Å) [N II] $\lambda 5755$, C IV $\lambda 5801$ and C IV $\lambda 5812$, He II $\lambda 5869$ and He I $\lambda 5876$. Also the broad Wolf-Rayet bump C IV was fitted with the center at $\lambda 5805$.

and red (5750–5900 Å) WR bumps as it is shown on Figure 3. We attempted to confirm the detection of broad WR features in our StWr 2-21 spectrum, and if possible to infer their properties.

The analysis methods used are the same as those described in Section 2.2. A local underlying continuum at all the studied regions was defined for the total spectrum using the algorithm from Shergin et al. (1996). The continuum-subtracted spectral region of each studied spectral region was fitted simultaneously as a blend of a single wide and many narrow Gaussian features. Wavelengths of the narrow Gaussian features used were selected from the list of emission lines located at the respective spectral regions. This list was created by the authors and used by programs described in Section 2.2 for automatic measuring of emission lines. The exact wavelengths of the narrow emission lines were kept fixed during the fitting procedure. During this procedure, the FWHMs of most narrow emission lines were equal to each other, and equal to the FWHM of the strongest

narrow emission line observed in the studied region, namely He II $\lambda 4686$ for the blue WR bump spectral region and He I $\lambda 5876$ for the red WR bump region. The FWHM of the strongest narrow emission line, the FWHM of the broad component and its position, and the intensities of all emission lines were used as free parameters during the fitting procedure. Any Gaussian feature was formally detected if the derived intensity was greater than the total error found for this line (Signal-to-Noise ratio > 1). Gaussian features with detected Signal-to-Noise ratios less than unity were excluded, and the fitting procedure was repeated.

The results from the fitting procedures and residuals are shown in Figure 3, while final intensities of all narrow emission lines are given in Table 2. It seems that the WR wide components are indeed present and have the following parameters resulting from the fitting procedure described above: (1) the broad component of the He II $\lambda 4686$ line (EW = 16 ± 5 Å, FWHM = 35 ± 15 Å, flux = $58 \cdot 10^{-16}$ ergs $s^{-1} cm^{-2}$); (2) the broad component of C IV centred at $\lambda 5805$ (EW = 9 Å, FWHM = 42 ± 3 Å, flux = $22 \cdot 10^{-16}$ ergs $s^{-1} cm^{-2}$). Our fitting method is too unstable in the region of the O VI $\lambda 3822$ feature, found previously by Zijlstra et al. (2006), to make any definitive conclusions of its existence in our data.

Both of the broad features which were found, and reported above, show the same velocity range of ≈ 2200 km s^{-1} . The resulting detected line ratio He II $\lambda 4686$ /C IV $\lambda 5805 \approx 2.6$ supports the conclusion of Zijlstra et al. (2006) that the central star of StWr 2-21 is a hot star midway between subclasses 2 and 3 ([WO 2-3]) according to the classification by Acker & Neiner (2003). The FWHMs of the detected broad lines also fit well those shown in Acker & Neiner (2003) for [WO 2-3] subclasses. No broad WR features were detected in the spectrum of BoBn 1 using the described fitting method.

Finally, four out of six PNe studied in dSphs (Walsh et al. 1997; Zijlstra et al. 2006; Kniazev et al. 2007; Larsen 2008, this work) show WR features in their spectra. This fraction (67%) is much higher than the fraction of [WR]-type central PNe stars in both the Galactic disk ($\sim 6.5\%$) and the Galactic bulge ($\sim 18\%$; Górny 2001; Górny et al. 2004). This high fraction of [WR]-type of central PNe stars, as noted by Zijlstra et al. (2006), supports models in which the probability of star to develop a WR wind is determined by parameters of the progenitor star rather than models where this occurrence is a random event caused by a late thermal pulse (Gesicki et al. 2006).

4 DISCUSSION

4.1 Additional Enrichment in PN Progenitors

H II region abundances mainly provide information about α -process elements, which are produced predominantly in short-lived massive stars. Because of their common origin, $\log(Ne/O)$, $\log(S/O)$ and $\log(Ar/O)$ should be constant and show no dependence on the oxygen abundance. Izotov & Thuan (1999) very accurately measured these α -element-to-oxygen abundance ratios in a large sample of H II regions in blue compact galaxies. They found that $\log(Ne/O) = -0.72 \pm 0.06$, $\log(S/O) = -1.55 \pm 0.06$ and

$\log(Ar/O) = -2.27 \pm 0.10$, as shown in Figure 4. Recent spectrophotometric results of Izotov et al. (2006) for a large sample of H II galaxies from the Sloan Digital Sky Survey DR3 data (Abazajian et al. 2005) support this conclusion. In addition, they found no significant trends with the oxygen abundance for the $\log(Cl/O)$ ratio. Using their published data we calculated weighted mean for the $\log(Cl/O)$ ratio as -3.46 ± 0.14 and plot these data in the bottom panel of Figure 4.

In contrast to H II regions, some elemental abundances in PNe are affected by the nucleosynthesis in the PN progenitors. Newly synthesized material can be dredged up by convection in the envelope, significantly altering abundances of He, C, and N in the surface layers during the evolution of the PN progenitor stars on the giant branch and asymptotic giant branch (AGB). Also a certain amount of oxygen can be mixed in during the thermally pulsing phase of AGB evolution (Kingsburg & Barlow 1994; Péquignot et al. 2000; Leisy & Dennefeld 2006). In combination, it means that only the Ne, S, Cl and Ar abundances, observed in both H II regions and PNe, can be considered as reliable probes of the enrichment history of galaxies, unaffected by the immediately preceding nucleosynthesis in the progenitor stars. Kniazev et al. (2005) compared observed α -element-to-oxygen abundance ratios to ones for H II regions, to estimate additional enrichment in oxygen for Type I PN in the nearby galaxy Sextans A. These authors found significant self-pollution of the PN progenitor, by a factor of ~ 10 in oxygen. Kniazev et al. (2007) used the same idea during a study of PN in the Fornax dSph galaxy and found that systematically lower ratios for $\log(S/O)$, $\log(Ar/O)$ and $\log(Ne/O)$ in this nebula can be easily explained with additional enrichment in oxygen by 0.27 ± 0.10 dex. After correction for this additional enrichment, all studied ratios increased to the values defined for H II regions, as shown in Figure 4. This conclusion is additionally supported by the fact that using the same correction for the observed $\log(Cl/O)$ ratio in the Fornax PN, moved the value to -3.41 , consistent with the H II regions (see panel (d) of Figure 4).

BoBn 1 in Sgr has a complicated abundance pattern, which are hard to show in Figure 4, since the differences are about 0.9 dex for $\log(S/O)$, $\log(Ar/O)$ and $\log(Cl/O)$ ratios but -0.9 dex for $\log(Ne/O)$. We will try to explain neon overabundance for BoBn 1 in Section 4.3 below. However, to explain the lower $\log(S/O)$, $\log(Ar/O)$ and $\log(Cl/O)$ ratios it is natural to suggest just an additional enrichment in oxygen, following Péquignot et al. (2000) and Kniazev et al. (2005, 2007). Using the abundance ratios for H II regions and our observed ratios, this self-pollution can be calculated as the weighted average, $\delta O = 1.09 \pm 0.13$ dex. After the correction the resulting oxygen abundance $12 + \log(O/H)$ is 6.72 ± 0.16 dex, that is, 1/110 the solar value (Lodders 2003), similar to the metallicity of the old globular cluster Terzan 8 in Sgr (Da Costa & Armandroff 1995). The corrected ratios (shown in Figure 4 as open circles) are $\log(S/O)_{\text{corr}} = -1.54 \pm 0.11$, $\log(Ar/O)_{\text{corr}} = -2.25 \pm 0.12$ and $\log(Cl/O)_{\text{corr}} = -3.62 \pm 0.23$, consistent with the values in H II regions, showing that a change in oxygen suffices. Finally, we can estimate that the PN progenitor in BoBn 1 enriched the ejecta by a factor of ~ 12 in oxygen and by a factor of ~ 240 in nitrogen.

Three of five PNe in dSph galaxies show observed

$\log(\text{Ne}/\text{O})$, $\log(\text{S}/\text{O})$, $\log(\text{Ar}/\text{O})$ and $\log(\text{Cl}/\text{O})$ ratios consistent with abundance ratios for H II regions. This implies that oxygen dredge-up affects abundances only under some circumstances. Richer & McCall (2007) analysed the abundances for the sample of bright PNe in dwarf irregular galaxies and also suggested that oxygen is dredged up on occasion, even at very low metallicity. Péquignot et al. (2000) argue that oxygen is a byproduct of all third dredge-up, but leads to enrichment only at low metallicity. At solar metallicity, the dredged-up material has *lower* oxygen abundance than the original gas.

It is uncertain why BoBn 1 would show a 3rd dredge-up (as evidenced by its carbon-rich nature) while other PNe at similar extreme abundances do not. Rotational mixing might be a reason (Siess, Goriely & Langer 2004). However, if BoBn 1 is a member of Sgr, it can have a younger age and larger progenitor mass than Galactic stars of the same metallicity, which favours the occurrence of 3rd dredge-up.

4.2 Abundance Comparison

Table 6 shows the elemental abundance of all known PNe in dSphs relative to the solar abundance of Lodders (2003). Values for He 2-436 and Wray 16-423 are from Dudziak et al. (2000), and for the Fornax PN from Kniazev et al. (2007). Dudziak et al. (2000) found that the abundances of the first two Sgr PNe are identical within their uncertainties (0.05 dex), which provides evidence that their progenitor stars formed in a single star burst event within a well-mixed ISM. This star formation episode is estimated to have taken place 5 Gyr ago (Zijlstra et al. 2006). StWr 2-21 shows significantly higher abundances and likely dates from a more recent event of star formation. All four objects are strongly enriched in carbon, with C/O ratios between 3 and 29.

We find that StWr 2-21 is the most metal-rich PN known for the dwarf spheroidal galaxies. Its [O/H] is similar to that of the few most metal-rich PNe in the LMC (Leisy & Dennefeld 2006). It confirms the existence of a metal-rich population in Sgr (Zijlstra et al. 2006), in good agreement with what was found by the spectroscopic analysis of red giants (Bonifacio et al. 2004; Monaco et al. 2005; Sbordone et al. 2007). The lack of nitrogen enrichment shows that the initial mass of the progenitor star was $M_i < 2.5 M_\odot$ and therefore puts a lower limit to the age of $t > 1$ Gyr. The N/O versus N/H abundance ratio of StWr 2-21 closely follows the relation for Galactic PNe (Leisy & Dennefeld 2006).

BoBn 1 is, in contrast, the most metal-poor object with well-determined abundances, in Sgr. Zijlstra et al. (2006) argue, based on limited data, that its original abundance was $[\text{Fe}/\text{H}] < -2$. We find slightly higher values, with S, Ar, Cl and Fe uniformly indicating an original metallicity of $[\text{Fe}/\text{H}] = -1.9$. The low metallicity indicates that it belongs to the old population of Sgr (see also the discussion in Bellazzini et al. 1999). The C/O = 25 is notable, showing that the nebular abundances are affected by extreme self-enrichment. In addition to C, this is also the case for N, O, and, surprisingly, for Ne.

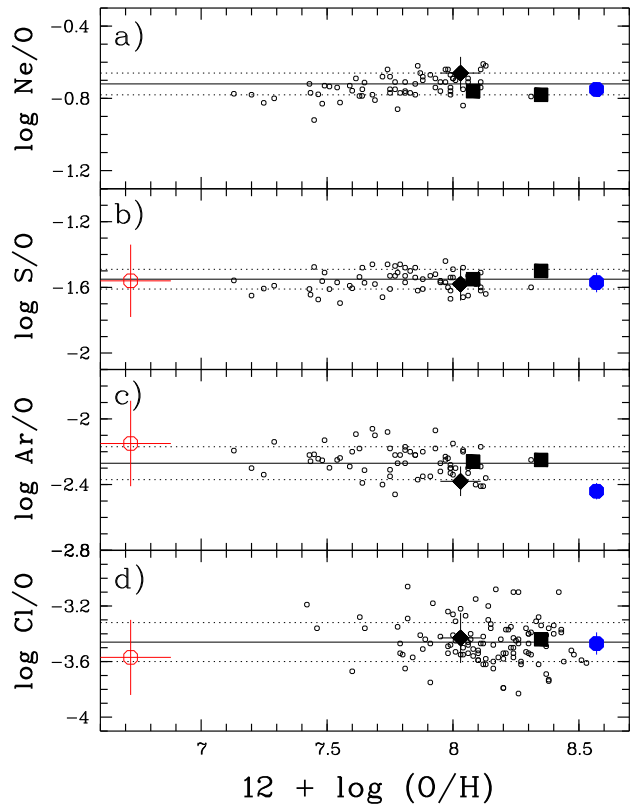


Figure 4. α -element-to-oxygen abundance ratios for $\log(\text{Ne}/\text{O})$, $\log(\text{S}/\text{O})$, $\log(\text{Ar}/\text{O})$ and $\log(\text{Cl}/\text{O})$ for H II regions with their 1σ errors (short-dashed lines) as a function of oxygen abundance (Izotov & Thuan 1999; Izotov et al. 2006). Data from Izotov & Thuan (1999); Kniazev et al. (2003); Izotov et al. (2006) are overplotted. Data for PNe in Fornax (filled diamond) and in the Sagittarius dSph galaxies are shown with their 1σ errors. Ratios for PN in Fornax are corrected for self-pollution in oxygen by 0.27 dex (Kniazev et al. 2007). Ratios shown for BoBn 1 in Sgr are corrected for self-pollution in oxygen by 1.09 dex as discussed in Section 4.1, and are plotted as open circles. Data for StWr 2-21 from current work are plotted as filled circles. Data for two PNe in the Sagittarius dSph galaxy from Walsh et al. (1997) were recalculated in the same way as described in Section 2.3 and are plotted as filled squares.

4.3 The Neon Problem

BoBn 1 shows a very unusual abundance pattern, with neon more abundant by number than oxygen. Oxygen and neon are both produced in Type-II supernovae, where they are produced in a fixed ratio. The abundance ratio is $\text{Ne}/\text{O} \sim 0.18$ in a range of environments (Henry 1989; Izotov & Thuan 1999; Izotov et al. 2006; Leisy & Dennefeld 2006), in confirmation of their common origin. Neon is also produced in carbon burning high-mass AGB stars and in high-mass novae, but not in amounts exceeding oxygen. However, significant neon can be produced in the inter-shell of low-mass AGB stars, and this is the likely origin of the enrichment in BoBn 1. In the large sample of Leisy & Dennefeld (2006), the Ne/O ratio is always less than unity: BoBn 1 is unique, and either shows the result of a

Table 6. Comparison of abundances

Element	Wray 16–423	He 2–436	StWr 2-21	BoBn 1	Fornax	Solar ^a	W–☉	He–☉	St–☉	BB–☉	F–☉
He	11.03	11.03	11.03	11.00	10.97	10.99	+0.04	+0.04	+0.04	+0.09	–0.01
C	8.86	9.06	9.11	9.20	9.02	8.46	+0.40	+0.60	+0.65	+0.74	+0.56
N	7.68	7.42	7.74	7.64	7.04	7.90	–0.22	–0.48	–0.16	–0.10	–0.86
O	8.33	8.36	8.57	7.81	8.01	8.76	–0.43	–0.40	–0.19	–0.95	–0.75
Ne	7.55	7.54	7.82	7.91	7.38	7.95	–0.40	–0.41	–0.13	–0.04	–0.57
S	6.67	6.59	6.99	5.16	6.45	7.26	–0.59	–0.67	–0.27	–1.83	–0.81
Cl	4.89	...	5.10	3.14	4.60	5.33	–0.44	...	–0.23	–2.19	–0.73
Ar	5.95	5.78	6.12	4.57	5.65	6.62	–0.67	–0.84	–0.50	–2.05	–0.97
Fe	6.87	5.72	6.38	7.54	–0.67	–1.82	–1.16

Note: The abundances are given as $12 + \log X/H$.

^a Solar system abundances are from Lodders (2003).

rather unusual event, or traces evolution within a rare parameter range like mass and/or metallicity.

The intershell contains the ashes of the preceding hydrogen burning. Following helium ignition, this intershell becomes convective and experiences burning at $T \sim 3 \times 10^8$ K (Herwig 2005). The nitrogen is burned to ^{22}Ne via two α captures. In high mass stars, hot bottom burning destroys the neon, but in low-mass stars this does not occur and neon increases to 2% by mass (Herwig 2005).

Intershell material is usually exposed only in hydrogen-poor stars, which are likely to have lost their hydrogen layer in a very late thermal pulse. These show significant enhancement in Ne (Werner et al. 2004), in two cases also with low O/Ne. Interestingly, the two cases with low O/Ne also show surface hydrogen, although still with $H/He \sim 1$ by mass.

BoBn 1 shows no evidence for hydrogen depletion, or of a separate hydrogen-poor region, and is therefore probably not related to the hydrogen-poor stars. Its intershell products instead are visible due to dredge-up. The neon abundance in BoBn 1 is about 0.15% by mass, compared to 2% expected in the intershell. This suggests dilution by a factor of 15. Assuming an intershell mass of $\sim 10^{-2} M_{\odot}$ (Herwig 2005) we find that the envelope mass at the time of the mixing would have been $\sim 0.1 M_{\odot}$. Assuming an initial metallicity of the envelope of $0.01 Z_{\odot}$, we find that the final surface abundances of C, N, O, Ne are dominated by the intershell products, while the helium abundance remains dominated by the original envelope. This can consistently explain the observed abundances. The C/O ratio in the intershell is ~ 20 (Iben & MacDonald 1995), which approaches the value seen in BoBn 1.

5 CONCLUSIONS

The first scientific results based on SALT observations were published by O’Donoghue et al. (2006); Woudt et al. (2006) and Brosch et al. (2007), based on imaging data. In this paper we present the first spectrophotometric results obtained with SALT and RSS during their performance verification phase that emphasize the long-slit capabilities of the RSS for spectrophotometric observations. The quality of our data permits us to measure line ratios of elements not accessible in earlier studies. We measured the electron temperatures, the electron densities and element abundances for O, N, Ne,

Ar, S, Cl, Fe, C and He elements in two PNe in the Sagittarius dSph galaxy. These results are presented in several tables and plots. Based on the data and discussion presented in the paper, the following conclusions can be drawn:

1. We confirm that StWr 2-21 is the most metal-rich PN known in any dwarf spheroidal galaxies and has an oxygen abundance of $12 + \log(O/H) = 8.57 \pm 0.02$ dex. This $[O/H]$ shows that Sgr contains a younger stellar population with $[Fe/H] \approx -0.2$, in good agreement with spectroscopic abundance measurements in Sgr stars. The element abundance ratios of Ne, S, Ar and Cl to O for StWr 2-21 are consistent with the expected patterns in H II regions showing absence of any additional enrichment in oxygen in the PN progenitor. The lack of nitrogen enrichment puts a lower limit to the age of PN progenitor $t > 1$ Gyr.

2. We obtain an oxygen abundance of $12 + \log(O/H) = 7.81 \pm 0.09$ for BoBn 1. According to our analysis, this value should be corrected downward by 1.09 ± 0.13 dex due to the self-pollution of oxygen by the PNe progenitor. After this correction the element abundance ratios S/O, Ar/O and Cl/O appear in a good overall accord with the trends seen for H II regions. This implies that the PN progenitor had an oxygen abundance of $12 + \log(O/H) = 6.72 \pm 0.16$ dex, or $1/110$ of the solar value, similar to the metallicity of the old globular cluster Terzan 8 in Sgr (Da Costa & Armandroff 1995). BoBn 1 is therefore one of the most metal-poor PNe with well-determined abundances and belongs to the old population of Sgr. During its normal stellar evolution, the PN progenitor enriched the material by a factor of ~ 12 in oxygen and by a factor of ~ 240 in nitrogen.

3. BoBn 1 shows a very unusual pattern with neon being more abundant by number than oxygen. This neon enrichment could be explained by production of neon in the intershell of low-mass AGB stars. In this case the final surface abundances of C, N, O, Ne are dominated by the intershell products, that can consistently explain the observed abundances.

4. We confirm the existence of Wolf-Rayet broad lines in StWr 2-21, but no WR features were detected in the spectrum of BoBn 1. The fraction of [WR]-type central PNe stars is 67% for dSph galaxies, that supports models in which the probability of star to develop a WR wind is determined by parameters of the progenitor star.

ACKNOWLEDGMENTS

We thank the anonymous referee for comments which improved the presentation of the manuscript. This paper was written while AAZ was a sabbatical visitor at the South African Astronomical Observatory in Cape Town; AAZ is grateful for the hospitality. We are grateful for the support of numerous people during the SALT PV phase. L.S.P. acknowledges the partial support of the Cosmomicrophysics program of the National Academy of Sciences and Space Agency of Ukraine.

REFERENCES

Abazajian, K., et al. 2005, *AJ*, 129, 1755
 Acker, A., & Neiner, C. 2003, *A&A*, 403, 659
 Aller, H.L., 1984, *Physics of Thermal Gaseous Nebulae*, Dordrecht, Reidel
 Baldwin, J.A., & Stone, R.P.S. 1984, *MNRAS*, 206, 241
 Barker, T. 1980, *ApJ*, 237, 482
 Bellazzini, M., Ferraro, F.R., & Buonanno, R. 1999, *MNRAS*, 304, 633
 Benjamin, R.A., Skillman, E.D., & Smith, D.P. 2002, *ApJ*, 569, 288
 Bonifacio, P., et al. 2004, *A&A*, 414, 503
 Brocklehurst, M. 1971, *MNRAS*, 153, 471
 Brocklehurst, M. 1972, *MNRAS*, 157, 211
 Brosch, N., Kniazev, A. Buckley, D. et al. 2007, *MNRAS*, submitted (astro-ph/0707.2150)
 Buckley, D.A.H., Swart, G.P., Meiring, J.G., 2006, *SPIE*, 6267
 Burgh, E.B., Nordsieck, K.H., Kobulnicky, H.A., Williams, T.B., O'Donoghue, D., Smith, M.P., Percival, J.W., 2003, *SPIE*, 4841, 1463
 Da Costa, G.S., & Armandroff, T.E. 1995, *AJ*, 109, 2533
 Danziger, I.J., Dopita, M.A., Hawarden, T.G., & Webster, B.L. 1978, *ApJ*, 220, 458
 Davey, A.R., Storey, P.J., & Kisielius, R. 2000, *A&AS*, 142, 85
 Dohm-Palmer, R.C. et al. 2001, *ApJ*, 555, L37
 Dudziak, G., Péquignot, D., Zijlstra, A.A., & Walsh, J.R. 2000, *A&A*, 363, 717
 Galavís M.E., Mendoza C., & Zeppen C.J., 1997, *A&AS*, 123, 159
 Gesicki, K., Zijlstra, A. A., Acker, A., Górny, S. K., Gozdziwski, K., & Walsh, J. R. 2006, *A&A*, 451, 925
 Górny, S.K. 2001, *Ap&SS*, 275, 67
 Górny, S.K., Stasińska, G., Escudero, A.V., & Costa, R.D.D. 2004, *A&A*, 427, 231
 Grebel, E. K., Gallagher, J. S., III, & Harbeck, D. 2003, *AJ*, 125, 1926
 Helmi, A., & White, S.D.M. 2001, *MNRAS*, 323, 529
 Henry R.B.C., 1989, *MNRAS*, 241, 453
 Herwig F., 2005, *ARA&A*, 43, 435
 Howard, J.W., Henry, R.B.C., & McCartney, S. 1997, *MNRAS*, 284, 465
 Hudson C.E., & Bell K.L., 2005, *A&A*, 430, 725
 Ibata, R.A., Gilmore, G., & Irvin, M.J. 1994, *Nature*, 370, 194
 Ibata, R.A., Gilmore, G., & Irvin, M.J. 1995, *MNRAS*, 277, 781
 Iben I., Jr., & MacDonald J., 1995, *LNP*, 443, 48
 Izotov, Y.I., & Thuan, T.X. 1998, *ApJ*, 500, 188
 Izotov, Y.I. & Thuan, T.X. 1999, *ApJ*, 511, 639
 Izotov, Y.I. & Thuan, T.X. 2004, *ApJ*, 602, 200
 Izotov, Y.I., Thuan, T.X., & Lipovetsky, V.A. 1994, *ApJ*, 435, 647
 Izotov, Y.I., Thuan, T.X., & Lipovetsky, V.A. 1997, *ApJS*, 108, 1
 Izotov, Y.I., Stasińska, G., Meynet, G., Guseva, N.G., & Thuan, T.X. 2006, *A&A*, 448, 955
 Kingsburg, R.L., & Barlow, M.J. 1994, *MNRAS*, 271, 257
 Kingsburg, R.L., & English, J. 1992, *MNRAS*, 259, 635
 Kniazev, A.Y., Pustilnik S.A., Masegosa J., et al. 2000, *A&A*, 357, 101
 Kniazev, A.Y., Grebel, E.K., Hao, L., Strauss, M., Brinkmann, J. & Fukugita, M. 2003, *ApJ*, 593, L73
 Kniazev, A.Y., Pustilnik, S.A., Grebel, E.K., Lee, H., & Pramskij, A.G. 2004, *ApJS*, 153, 429
 Kniazev, A.Y., Grebel, E.K., Pustilnik, S.A., Pramskij, A.G., & Zucker, D. 2005, *AJ*, 130, 1558
 Kniazev A.Y., Grebel, E.K., Pustilnik, S.A., & Pramskij, A.G. 2007, *A&A*, 468, 121
 Kobulnicky, H.A., Nordsieck, K.H., Burgh, E.B., Smith, M.P., Percival, J.W., Williams, T.B., O'Donoghue, D., 2003, *SPIE*, 4841, 1634
 Koch, A., Wilkinson, M.I., Kleyna, J.T., Gilmore, G.F., Grebel, E.K., Mackey, A.D., Evans, N.W., & Wyse, R.F.G. 2007a, *ApJ*, 657, 241
 Koch, A., Grebel, E.K., Kleyna, J.T., Wilkinson, M.I., Harbeck, D.R., Gilmore, G.F., Wyse, R.F.G., & Evans, N.W. 2007b, *AJ*, 133, 270
 Kwitter, K.B., & Henry, R.B.C. 1996, *ApJ*, 473, 304
 Larsen, S.S., 2008, *A&A*, 477, L17
 Layden, A.C., & Sarajedini, A. 1997, *ApJ*, 486, L107
 Layden, A.C., & Sarajedini, A. 2000, *AJ*, 119, 1760
 Leisy P., Dennefeld M., 2006, *A&A*, 456, 451
 Liu, X.-W. 2003, in *Planetary Nebulae*, ed. S. Kwok, M. Dopita, R. Sutherland (San Francisco: ASP), *IAU Symp.*, 209, 339
 Liu, X.-W., Storey, P.J., Barlow, M.J., et al. 2000, *MNRAS*, 312, 585
 Liu, X.-W., Luo, S.-G., Barlow, M.J., Danziger, I.J., & Storey, P.J. 2001, *MNRAS*, 327, 141
 Lodders, K. 2003, *ApJ*, 591, 1220
 Majewski, S.R., Skrutskie, M.F., Weinberg, M.D., & Osthheimer, J.C. 2003, *ApJ*, 599, 1082
 Massey, P., Strobel, K., Barner, J.V., & Anderson, E. 1988, *ApJ*, 328, 315
 Marconi, G. et al. 1998, *A&A*, 330, 453
 Monaco, L., et al. 2004, *MNRAS*, 353, 874
 Monaco, L., Bellazzini, M., Bonifacio, P., Ferraro, F.R., Marconi, G., Pancino, E., Sbordone, L., & Zaggia, S. 2005, *A&A*, 441, 141
 Newberg, H. J., et al. 2003, *ApJL*, 596, L191
 Nussbaumer, H., & Storey, P.J., 1984, *A&AS*, 56, 293
 O'Donoghue, D., et al. 2006, *MNRAS*, 372, 151
 Oke, J.B. 1990, *AJ*, 99, 1621
 Peña, M., Torres-Peimbert, S. & Ruiz, M.T. 1991, *PASP*, 103, 865
 Péquignot, D., Petitjean, P., & Boisson, C. 1991, *A&A*, 251, 680
 Péquignot, D., Walsh, J. R., Zijlstra, A. A., & Dudziak, G.

- 2000, *A&A*, 361, L1
Pilyugin L.S., 2007, *MNRAS*, 375, 685
Putman, M.E., Thom, C., Gibson, B.K., & Staveley-Smith, L. 2004, *ApJ*, 603, L77
Richer, M.G., & McCall, M.L. 2007, *ApJ*, 658, 328
Sbordone, L. et al. 2007, *A&A*, 465, 815
Shergin, V.S., Kniazev, A.Y., & Lipovetsky, V.A. 1996, *Astronomische Nachrichten*, 2, 95
Siess, L., Goriely, S., & Langer, N., 2004, *A&A*, 415, 1089
Stanghellini, L., & Kaler, J.B. 1989, *ApJ*, 343, 811
Stasińska, G. 2005, *A&A*, 434, 507
Stone, R.P.S., & Baldwin, J.A. 1983, *MNRAS*, 204, 347
Torres-Peimbert, S., & Peimbert, M. 1979, *Revista Mexicana de Astronomia y Astrofisica*, 4, 341
Walsh, J.R., Dudziak, G., Minniti, D., & Zijlstra, A.A. 1997, *ApJ*, 487, 651
Werner K., Rauch T., Reiff E., Kruk J. W., & Napiwotzki R. 2004, *A&A*, 427, 685
Whitford, A.E. 1958, *AJ*, 63, 201
Woudt P.A., et al. 2006, *MNRAS*, 371, 1497
Wright, S.A., Corradi, R.L.M., & Perinotto, M. 2005, *A&A*, 436, 967
Zijlstra, A.A. & Walsh, J.R. 1996, *A&A*, 312, L21
Zijlstra, A.A., Gesicki, K., Walsh, J. R., Péquignot, D., van Hoof, P. A. M., & Minniti, D. 2006, *MNRAS*, 369, 875

This paper has been typeset from a \TeX / \LaTeX file prepared by the author.